Comparison of inelastic neutrino and antineutrino scattering on nuclei

E. Kolbe and K. Langanke
Institut für Theoretische Physik I, Universität Münster, W-4400 Münster, Germany

S. Krewald
Institut für Kernphysik, Forschungszentrum Jülich, W-5170 Jülich, Germany
(Received 26 November 1991)

Based on calculations performed with the continuum random phase approximation model we compare neutrino- and antineutrino-induced reactions on several target nuclei. We find that neutrinos and antineutrinos excite parts of the isovector giant dipole resonance differently, with scattering on ^{16}O showing the most noticeable deviations.

PACS number(s): 25.30.Pt, 24.80.Ba

The study of semileptonic weak interactions in nuclei has been pioneered by Donnelly and Walecka ([1,2] and references therein). Besides the fundamental theoretical aspect to confirm the structure of the weak neutral current [3–5], inelastic neutrino scattering experiments were proposed to serve as a probe for nuclear structure and especially were proclaimed to be, in principle, a richer source of information than electron scattering experiments, because axial vector currents contribute to the interaction in addition to the vector currents. It is one aim of this paper to give an explicit example (the regime of the isovector giant dipole resonance) where neutrino scattering is expected to give more insight into nuclear structure than standard electron scattering experiments.

The interest in semileptonic weak interactions has recently also been motivated by some practical applications: Inelastic neutrino and antineutrino scattering on nuclei are expected to be an important background contribution to the detector system developed for the Los Alamos neutrino oscillation experiment [3]. With relevance to this application, we have calculated the (ν_e, e^-), (ν_e, ν_e'), and $(\bar{\nu}_\mu, \bar{\nu}_\mu')$ cross sections for the target nuclei ^{12}C and ^{16}O as a function of excitation energy. In the energy regime dominated by the isovector giant dipole resonance (GDR) we find noticeable differences between the inelastic neutrino and antineutrino cross sections. In particular, our calculation predicts that from the well-known double-bump structure of the isovector GDR in ^{16}O, as observed in reactions with unpolarized electrons [6] or in the photoabsorption cross section [7], only the lower resonant structure is excited by antineutrino scattering, while neutrino-induced reactions excite the other part of the GDR. These differences will be related to the particle-hole structure of the final states.

In the following we want to substantiate this prediction by results obtained within an investigation of inelastic neutrino/antineutrino-induced reactions on selected $T=0$ target nuclei studied within the framework of the continuum random phase approximation (continuum RPA). As the theoretical background has been outlined in Refs. [8,9], a brief discussion of the main ingredients of our calculation suffices here.

For our problem at hand, the $T=1$ continuum can only be excited by the isovector part of the weak Hamiltonian. Assuming a current-current form for this operator,

$$H^{\rm cc}=\frac{g}{\sqrt{2}}(j_\lambda^{(+)}J^{(-)\lambda}+j_\lambda^{(-)}J^{(+)\lambda}) , \tag{1}$$

we have

$$j_\lambda^{(-)}=\bar{\Psi}_e\gamma_\lambda(1-\gamma_5)\Psi_{\nu_e} , \tag{2}$$

$$J_\lambda^{(+)}=\bar{\Psi}_p[g_1^V(q^2)\gamma_\lambda+g_2^V(q^2)i\sigma_{\lambda\nu}q^\nu + g_1^A(q^2)\gamma_\lambda\gamma_5]\Psi_n , \tag{3}$$

for the leptonic and hadronic charged currents ($j_\lambda^{(+)}, J_\lambda^{(-)}$ are their Hermitian conjugates) and

$$j_\lambda^{(0)}=\bar{\Psi}_{\nu_e}\gamma_\lambda(1-\gamma_5)\Psi_{\nu_e} , \tag{4}$$

$$J_\lambda^{(0)}=J_\lambda^{V_3}-2\sin^2\Theta_W J_\lambda^{\rm em} , \tag{5}$$

$$J_\lambda^{V_3}=\bar{\Psi}_{p,n}[g_1^V(q^2)\gamma_\lambda+g_2^V(q^2)i\sigma_{\lambda\nu}q^\nu + g_1^A(q^2)\gamma_\lambda\gamma_5]\Psi_{p,n} , \tag{6}$$

for the neutral currents, with similar contributions to the leptonic currents arising from the other neutrino flavors. $J_\lambda^{\rm em}$ is the isovector part of the electromagnetic current. The various nucleon form factors $g_{1,2}^V$ and g^A are known from electron scattering and β decay at $q^2=0$. Their q^2 dependence is well described by a dipole form whose parameters we adopted from Ref. [10]. For the Weinberg angle we used $\sin^2\Theta_W=0.233$.

Following Walecka [2], the cross sections for neutrino/antineutrino-induced reactions from an initial to a final nuclear state with quantum numbers $\{J_i\}$ and $\{J_f\}$, respectively, are given by

$$\left[\frac{d^2\sigma_{i\to f}}{d\Omega_e d\omega}\right]_{\nu/\bar{\nu}} = \frac{g^2\epsilon_f^2}{2\pi^2}\frac{4\pi\cos^2\Theta/2}{(2J_i+1)}F(Z,\epsilon_f)\left[\sum_{J=0}^{\infty}\sigma_{CL}^J+\sum_{J=1}^{\infty}\sigma_T^J\right],$$

$$\sigma_{CL}^J = |\langle J_f\|\tilde{M}_J(q)+(w/|\vec{q}|)\tilde{L}_J(q)\|J_i\rangle|^2 , \tag{7}$$

$$\sigma_T^J = \left[-\frac{q_\mu^2}{2\vec{q}^2}+\tan^2\frac{\Theta}{2}\right]\times\left[|\langle J_f\|\tilde{J}_J^{\rm mag}(q)\|J_i\rangle|^2+|\langle J_f\|\tilde{J}_J^{\rm el}(q)\|J_i\rangle|^2\right]$$
$$\mp\tan\frac{\Theta}{2}\left[-\frac{q_\mu^2}{|\vec{q}|^2}+\tan^2\frac{\Theta}{2}\right]^{1/2}\times\left[2\,{\rm Re}\langle J_f\|\tilde{J}_J^{\rm mag}(q)\|J_i\rangle\langle J_f\|\tilde{J}_J^{\rm el}(q)\|J_i\rangle^*\right].$$

Here g is the universal coupling constant, Θ the angle between the incoming and outgoing lepton, and $q_\mu=(w,\vec{q})(q:=|\vec{q}|)$ the four-momentum transfer. The quantities $\tilde{M}_J,\tilde{L}_J,\tilde{J}_J^{\rm el}$, and $\tilde{J}_J^{\rm mag}$ denote the multipole operators for the charge, and the longitudinal and transverse electric and magnetic parts of the four-current, respectively [2]. The final-state interaction between the outgoing electron and the nucleus is accounted for by the Coulomb function $F(Z,\epsilon)$ [11]. The interference term in (7) does not vanish due to the parity-breaking axial vector component in the transverse electric and magnetic multipole operators. The different signs of these terms for neutrino- and antineutrino-induced reactions stems from the opposite helicities of neutrinos and antineutrinos, where the minus sign refers to the neutrino cross section. In the following we will discuss our results in terms of the "total cross section" $\sigma(\omega)$ obtained by integrating (7) over the angle Θ.

We calculate the nuclear many-body states within the continuum RPA model [8,9]. As with the residual particle-hole interaction we adopt the finite-range force of Ref. [12] derived from the Bonn meson-exchange potential [13]. To test the sensitivity of our results on the used interaction we have performed additional calculations adopting the zero-range Landau-Migdal force [14] as well as this interaction with an effective mass parameter $m^*=0.9$ [15]. As our calculations yield qualitatively the same results for all residual interactions, we will in the following only present cross sections calculated for the finite-range force.

At first we assumed a fixed neutrino/antineutrino energy of $E_\nu=29.8$ MeV, corresponding to the monoenergetic muon neutrinos emerging from π^+ decay at rest, for this allows an investigation of possible differences in the inelastic neutrino and antineutrino scattering cross sections independently of the (for neutrinos and antineutrinos different) energy distributions in actual experiments.

Figure 1 shows the total neutral-current cross sections (upper part) as well as the dominant multipole contributions (lower part) for inelastic neutrino and antineutrino scattering on ^{16}O for excitation energies above the nucleon threshold. The energy scale in Fig. 1 refers to excitation energies in ^{16}O. In the energy regime below ≈ 30 MeV, the cross section is clearly dominated by resonances with $J^\pi=1^-$ and 2^-. Comparing the ν- and $\bar{\nu}$-induced reactions, we find that the cross sections show the same overall structure, with the noticeable exception of the energy regime between ≈ 20 and 28 MeV, which is dominated by the isovector GDR [16] (see Fig. 1). Here our calculation predicts that from the double-bump structure of the GDR with principal structures at $E=22.1$ and 24.1 MeV [16], antineutrino reactions only excite the lower resonance, while the upper part predom-

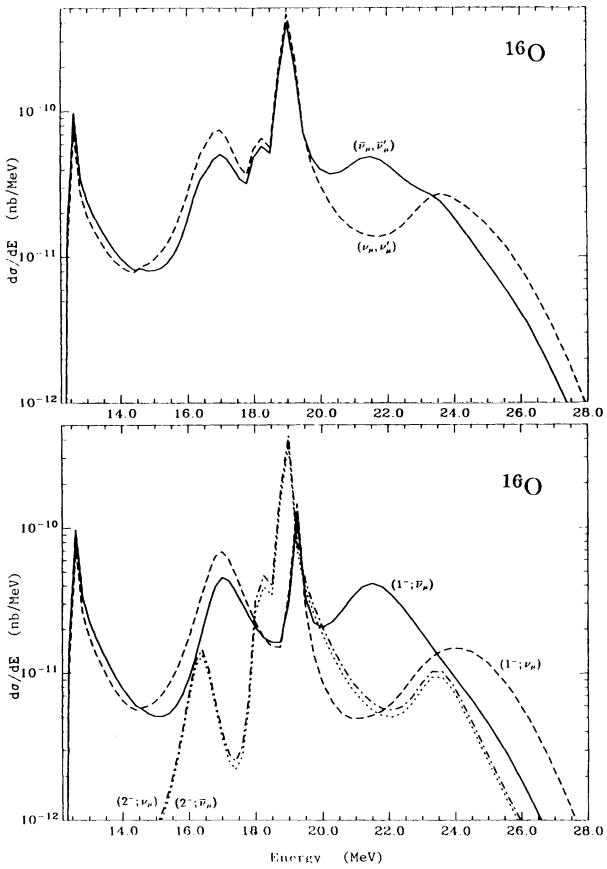

FIG. 1. (Upper part) Comparison of inelastic neutrino- and antineutrino-induced cross sections on ^{16}O calculated for a fixed neutrino energy $E_\nu=29.8$ MeV, ^{16}O$(\bar{\nu},\bar{\nu}')^{16}$O* (solid line), ^{16}O$(\nu,\nu')^{16}$O* (dashed line). (Lower part) The dominating multipole contributions to the cross sections are shown: $J^\pi=1^-$ (solid) and 2^- (dotted) contributions to the ^{16}O$(\bar{\nu},\bar{\nu}')^{16}$O* cross section, 1^- (dashed) and 2^- (dash-dotted) contributions to the ^{16}O$(\nu,\nu')^{16}$O* cross section.

inantly shows up in the neutrino-induced reaction cross sections. The small structure visible in the $(\bar{\nu},\bar{\nu}')$ cross section at around 24 MeV is due to a 2^- resonance, corresponding to the tentative experimental state at 23.7 ± 0.3 MeV [16].

To understand the predicted differences for the excitation cross sections in ν and $\bar{\nu}$ scattering we have performed a detailed analysis of the various multipole contributions. At first we observed that from the two components present in the interference term (transverse electric and magnetic) usually one dominates the other. Then the contribution to the total cross section due to the interference term is relatively small, and, as a consequence, the ν- and $\bar{\nu}$-induced cross sections are about equal. This argument holds also for the 1^- multipole contributions where, except for energies between ≈ 22 and 28 MeV, the matrix elements of the axial vector (magnetic) operator $\langle J_f \| J^m \| J_i \rangle$ are noticeably larger than those for the vector (electric) operator $\langle J_f \| J^e \| J_i \rangle$. However, at the two resonances ($E \approx 22$ and 25 MeV) the magnitude of the magnetic and electric matrix elements becomes about equal, giving rise to strong contributions from the interference term. Furthermore, $\langle J_f \| J^e \| J_i \rangle$ changes its sign at an energy $E \approx 23.5$ MeV between the two resonances. Consequently, we find destructive interference at the lower resonance and constructive interference at the upper resonance in ν scattering, while the interference pattern is opposite for $\bar{\nu}$ scattering.

The structure of a collective state in the continuum can be studied in terms of the weight of its different asymptotic decay channels. This is done in Fig. 2, where we have split the $J^\pi = 1^-$ cross section into the dominant contributions corresponding to different asymptotic decay channels. The plot is restricted to the energy regime $E > 18.4$ MeV, at which particles can be removed from the $p_{3/2}$ shell. One clearly observes that at the lower resonance mainly the $(d_{3/2})^{+1}(p_{1/2})^{-1}$, $(s_{1/2})^{+1}(p_{3/2})^{-1}$, and $(d_{5/2})^{+1}(p_{3/2})^{-1}$ channels contribute which all show a pronounced resonantlike maximum in $\bar{\nu}$ scattering, but not in ν scattering. The upper resonance is dominated by the $(d_{3/2})^{+1}(p_{3/2})^{-1}$ channel, which is resonant for ν and $\bar{\nu}$ scattering. However, in this decay channel the ν cross section is larger than the $\bar{\nu}$ cross section in the energy regime of interest, exceeding the latter by about a factor of 3 on top of the resonance. In agreement with the discussion given above we find that for all particle-hole contributions the matrix elements $\langle p \| J^m \| h \rangle$ are generally larger than those for the (vector) electric operator $\langle p \| J^e \| h \rangle$. The change of sign of $\langle J_f \| J^e \| J_i \rangle$ at $E \approx 23.5$ MeV is explained by the fact that the signs of the particle-hole contributions $\langle p \| J^e \| h \rangle$ are different for the $(d_{3/2})^{+1}(p_{3/2})^{-1}$ configuration (dominating the upper resonance) and the $(d_{3/2})^{+1}(p_{1/2})^{-1}$, $(s_{1/2})^{+1}(p_{3/2})^{-1}$ and the $(d_{5/2})^{+1}(p_{3/2})^{-1}$ configuration (dominating the lower resonance). Note that the nucleon spin is flipped in the $(d_{3/2})^{+1}(p_{3/2})^{-1}$ configuration, while there is no spin

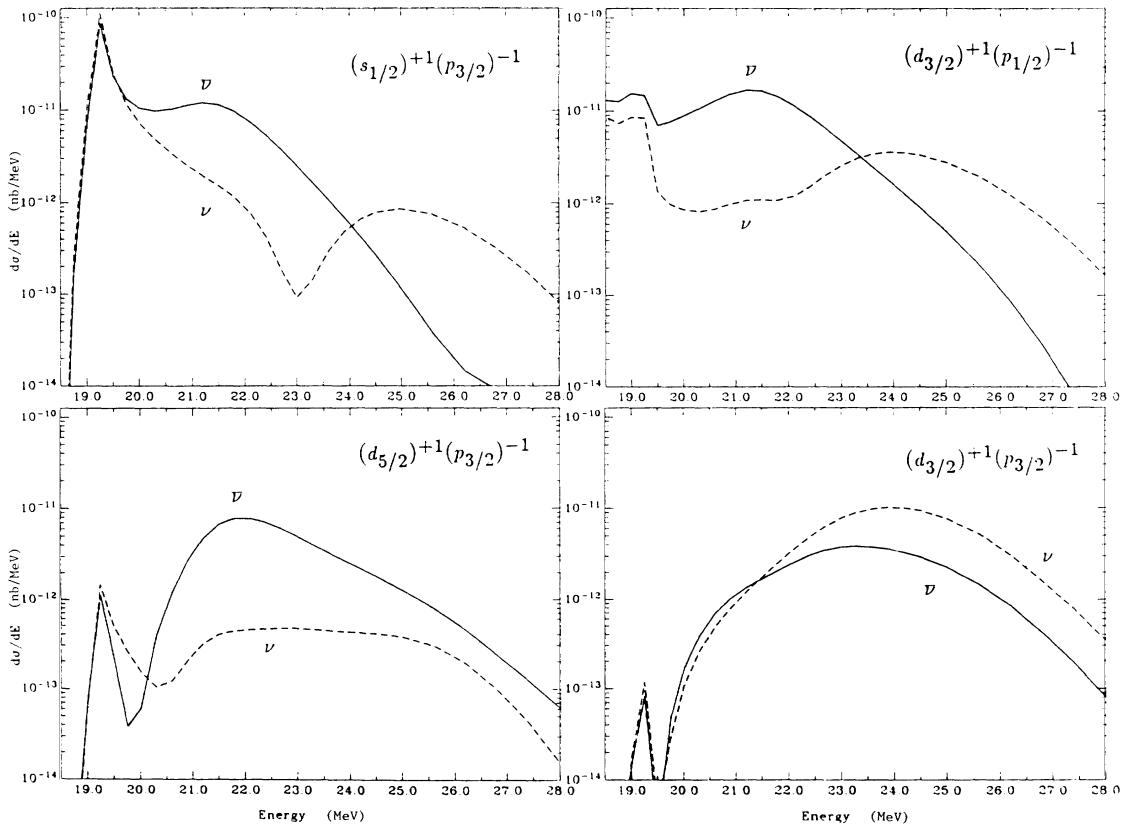

FIG. 2. Contributions of various asymptotic decay channels to the $J^\pi = 1^-$ part of the $^{16}O(\bar{\nu},\bar{\nu}')^{16}O^*$ (solid lines) and $^{16}O(\nu,\nu')^{16}O^*$ (dashed lines) cross sections in the range of the giant dipole resonance.

flip for the $(d_{3/2})^{+1}(p_{1/2})^{-1}$ and the $(d_{5/2})^{+1}(p_{3/2})^{-1}$ contributions. Thus, by being sensitive to the signs of the matrix elements $\langle J_f \| J^e \| J_i \rangle$ and $\langle J_f \| J^m \| J_i \rangle$ (which cannot be determined in standard electron-scattering experiments, where only the squared matrix elements enter into the cross section formula [17]) the comparison of neutrino/antineutrino cross sections might provide a richer experimental probe of the structure of the GDR.

Experiments which might be set up to look for this predicted difference in the $\nu/\bar{\nu}$ scattering on ^{16}O will likely use neutrino/antineutrino beams stemming from π decay (and the subsequent μ decay). While the ν_μ's emerging from π^+ decay at rest are monoenergetic ($E_{\nu_\mu}=29.8$ MeV), the ν_e's and $\bar{\nu}_\mu$'s have the well-known spectral distribution [18]:

$$n_{\nu_e}(E_{\nu_e})=\frac{96E_{\nu_e}^2}{m_\mu^4}(m_\mu-2E_{\nu_e}) , \tag{8}$$

$$n_{\bar{\nu}_\mu}(E_{\bar{\nu}_\mu})=\frac{32E_{\bar{\nu}_\mu}^2}{m_\mu^4}(\tfrac{3}{2}m_\mu-2E_{\bar{\nu}_\mu}) , \tag{9}$$

where m_μ is the μ mass in MeV. To estimate the cross sections for these experiments we fold $\sigma(\omega)$, defined in (7), with the distributions as given in (8), (9):

$$\bar{\sigma}(\omega)=\int_\omega^\infty \sigma(E_\nu,\omega)n(E_\nu)dE_\nu . \tag{10}$$

The (ν_μ,ν'_μ) cross section from Fig. 1 and the folded cross section $\bar{\sigma}(\omega)$ for the (ν_e,e^-),(ν_e,ν'_e), and $(\bar{\nu}_\mu,\bar{\nu}'_\mu)$ reactions on ^{16}O are compared in Fig. 3 clearly showing the differences in the excitation cross sections in the range of the isovector GDR. We conclude from Fig. 3 that the cross section for ν_μ-induced reactions (which can be distinguished from ν_e- and $\bar{\nu}_\mu$-induced reactions by timing [5]) is predicted to show a one-bump structure for excitation energies above $\approx$20 MeV, while the sum of the (ν_e,ν'_e) and $(\bar{\nu}_\mu,\bar{\nu}'_\mu)$ cross sections (ν_e- and $\bar{\nu}_\mu$-induced reactions cannot be distinguished by timing in the experimental setup of Ref. [5]) should have the double-bump structure known from electron scattering. Furthermore, the same one-bump structure as in (ν_μ,ν'_μ) scattering can be seen in the charged-current reaction ^{16}O$(\nu_e,e^-)^{16}$F*. As the latter cross section is considerably larger, its determination by the experiment should be easier.

Finally, we have studied ν- and $\bar{\nu}$-induced reactions on other target nuclei like ^{12}C, ^{28}Si, ^{32}S, and ^{40}Ca. In all cases we observed only (noticeable) differences between neutrino/antineutrino cross sections for the $J^\pi=1^-$ multipole excitations. For the three heavier nuclei, these effects will hardly be observable, as the cross sections are mainly dominated by 2^- excitations. For the reactions on ^{12}C, our calculation predicts a noticeably different cross section for inelastic (ν_μ,ν'_μ) and $(\bar{\nu}_\mu,\bar{\nu}'_\mu)$ scattering to the 1^- resonance at around 25 MeV (see Fig. 4), where the neutrino-induced cross section is calculated to be about 2.5 times larger. The dominating decay channel of this resonance is found to be $(d_{3/2})^{+1}(p_{3/2})^{-1}$, as in the

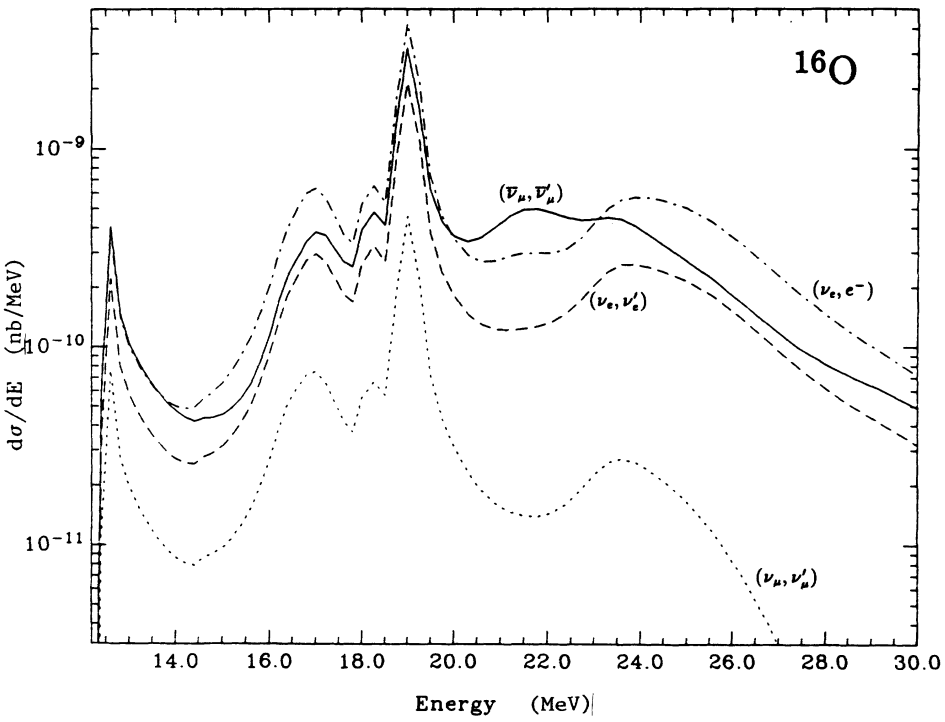

FIG. 3. ^{16}O$(\nu_e,\nu'_e)^{16}$O* (dashed line) and ^{16}O$(\bar{\nu}_\mu,\bar{\nu}'_\mu)^{16}$O* (solid line) cross sections calculated for the neutrino and antineutrino spectra defined in (8), (9). ^{16}O$(\nu_\mu,\nu'_\mu)^{16}$O* (dotted line) cross section for fixed neutrino energy $E_\nu=29.8$ MeV and charge current reaction ^{16}O$(\nu_e,e^-)^{16}$F* (dash-dotted line) cross section for the spectrum defined in (8). For the charged-current processes the energy scale can be transformed to the excitation energy in the final ^{16}F nucleus by subtracting 12.97 MeV.

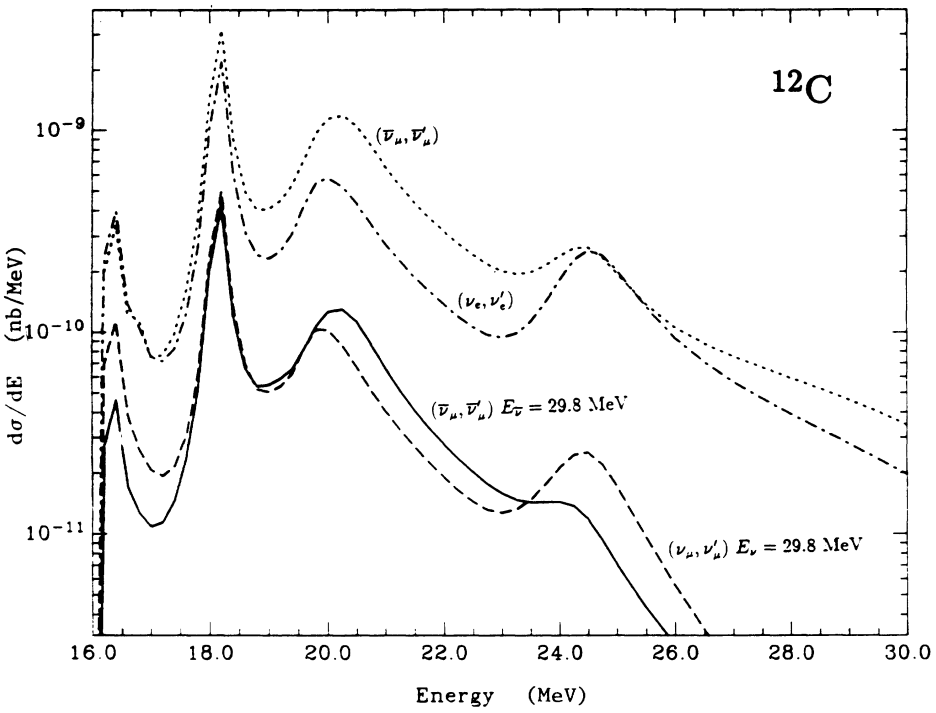

FIG. 4. Comparison of inelastic neutrino- and antineutrino-induced cross sections on ^{12}C. $^{12}C(\bar{\nu},\bar{\nu}')^{12}C^*$ (solid) and $^{12}C(\nu,\nu')^{12}C^*$ (dashed) are calculated for a fixed neutrino energy $E_\nu=29.8$ MeV. $^{12}C(\nu_e,\nu'_e)^{12}C^*$ (dash-dotted) and $^{12}C(\bar{\nu}_\mu,\bar{\nu}'_\mu)^{12}C^*$ (dotted line) cross sections are calculated for the neutrino and antineutrino spectra defined in (8), (9).

upper part of the GDR in ^{16}O. However, in actual experiments we expect this structure effect in the cross sections to be buried by the different energy dependences of the ν_e and $\bar{\nu}_\mu$ distributions (see Fig. 4).

In conclusion, we have studied neutrino/antineutrino scattering on selected nuclei, which is expected to be a likely background source in the detector system of the Los Alamos neutrino oscillation experiment. Our calculation shows noticeable differences between the neutrino- and antineutrino-induced cross sections in the regime of the isovector giant dipole resonance. We have argued that this effect is related to the spin structure of the GDR which becomes visible owing to the different helicities of neutrinos and antineutrinos. In principle, this effect might also be observed in polarized electron scattering. To be sensitive to the nuclear axial vector component (otherwise the interference term vanishes) one might either use a polarized target or an experiment in which a polarized particle ejected from the nucleus is detected in coincidence with the scattered electron. In the present case (spin-zero nuclei) $(\vec{e},e'\vec{p})$ experiments seem to be an alternative to neutrino/antineutrino scattering. Finally, our calculations indicate that neutrino scattering obviously offers a very rewarding, but experimentally extremely challenging tool to probe nuclear structure beyond the present possibilities [19].

[1] T. W. Donnelly and R. D. Peccei, Phys. Rep. **50**, 1 (1979).
[2] J. D. Walecka, in *Semileptonic Weak Interactions in Nuclei in Muon Physics,* edited by V. W. Hughes and C. S. Wu (Academic, New York).
[3] X. Q. Lu *et al.*, LAMPF Research Report No. LA-UR-89-3764, 1989.
[4] G. Drexlin *et al.*, KARMEN Collaboration, in *Proceedings of the Neutrino Workshop, Heidelberg, 1987,* edited by B. Povh and V. Klapdor (Springer-Verlag, Berlin, 1987), p. 147.
[5] G. Drexlin *et al.*, KARMEN Collaboration, Phys. Lett. B **267**, 321 (1991).
[6] N. Zimmermann *et al.*, *Physics with MAMI A* (Universität Mainz, 1988), p. 159.
[7] J. Ahrends *et al.*, Nucl. Phys **A251**, 479 (1975).
[8] M. Buballa, S. Drożdż, S. Krewald, and J. Speth, Ann. Phys. (N.Y.) **208**, 346 (1991).
[9] E. Kolbe, K. Langanke, S. Krewald, and F. K. Thielemann, Nucl. Phys. A (in print).
[10] E. J. Beise and R. D. McKeown, Comments Nucl. Part. Phys. **20**, 105 (1991).
[11] W. C. Haxton, G. J. Stephenson, Jr., and D. Strottman, Phys. Rev. D **25**, 2360 (1982).
[12] K. Nakayama, S. Drożdż, S. Krewald, and J. Speth, Nucl. Phys. **A470**, 573 (1987).
[13] R. Machleidt, K. Holinde, and Ch. Elster, Phys. Rep. **149**, 1 (1987).
[14] G. Co and S. Krewald, Nucl. Phys. **A433**, 392 (1985).

[15] M. Buballa, A. Gattone, R. DeHaro, R. Jessenberger, and S. Krewald, Nucl. Phys. **A517**, 61 (1990).
[16] F. Ajzenberg-Selove, Nucl. Phys. **A460**, 1 (1986).
[17] T. deForest and J. D. Walecka, Adv. Phys. **15**, 1 (1966).
[18] H. Ueberall, Nuovo Cimento **23**, 219 (1962).
[19] P. Schwandt, in *Proceedings of the International Nuclear Physics Conference,* edited by M. S. Hussein *et al.* (World-Scientific, Singapore, 1990), p. 133.